Multipath Cluster Fading Statistics and Modeling in Millimeter-Wave Radio Channels

Naveed Iqbal, *Student Member, IEEE*, Jian Luo, Robert Müller, Gerhard Steinböck, Christian Schneider, Diego Andres Dupleich, Stephan Häfner, Reiner S. Thomä, *Fellow, IEEE*

***Abstract*— The second-order statistics of indoor directional channels are investigated using millimeter-wave (mmWave) band (30.4–37.1 GHz) ultrawideband (UWB) channel measurements. Considering two main mmWave system assumptions (high bandwidth and high beamforming gain), this paper aims to investigate the validity of the Rayleigh–Rice fading models for the cluster fading envelope. The results from the mmWave band study are compared to an already well-studied lower frequency FCC band (3.4–10.1 GHz). During the measurements, only selective objects (emulated multipath clusters in the propagation channel) are illuminated in a small lecture room. The experiments show that for both UWB channels, the complex received (Rx) signal is a circularly symmetric non-Gaussian random variable with highly correlated inphase (I) and quadrature (Q) components. These properties demonstrate that the intracluster multipath components (MPCs) structure is sparse. Consequently, modeling the cluster fading envelope with Rayleigh–Rice distribution is not realistic. Therefore, the sum-of-cisoids principle is used for intracluster multipath modeling which inherently considers a correlation between I and Q components. It has been established that a reasonably good approximation of the cluster fading envelope can be obtained with $N = 3-6$ equal amplitude cisoids. However, we remark that Rayleigh–Rice models may become realistic cluster fading envelopes for narrowband mmWave systems.**

***Index Terms*— Channel modeling, millimeter-wave (mmWave) measurements, mmWave systems, multipath clusters, radio channels, small-scale fading, ultrawideband (UWB) channels.**

I. Introduction

CHANNEL models depend on system assumptions. Given the same propagation channel, systems with different properties—e.g., bandwidth and beamforming gain—may see different channel fading behavior [1]–[4]. Channel models should, thus, be capable of translating these effects when evaluated for a particular communication system. For example, 3GPP-LTE systems [5] apply spatial preprocessing and postprocessing to narrowband channels, and therefore, 3GPP-SCM [6] and WINNER [7] models are based on narrowband assumptions such as local-sense stationary and uncorrelated scattering of resolvable taps also known as clusters. Cluster amplitude fading envelope in 3GPP-SCM/WINNER models is modeled as a Rayleigh distributed random process.[1] Second-order statistics[2] of Rayleigh–Rice fading signals show that the Rx signal $\boldsymbol{Z} = \boldsymbol{X} + j\boldsymbol{Y}$ is a circularly symmetric complex Gaussian random process. It means that both real ($\boldsymbol{X}$) and imaginary ($\boldsymbol{Y}$) parts of $\boldsymbol{Z}$ are mutually uncorrelated Gaussian random variables having equal variances [8], [9]. This is justified by the central limit theorem which requires a superposition of an appreciable number of scattered/diffuse multipath components (MPCs) (N) [10]. Thus, Rayleigh and Rice fading models correspond to rich scattering channels and the same is true for Loo [11], Suzuki [12], and Nakagami [13] fading models.

Cluster fading envelopes modeled by the state-of-the-art millimeter-wave (mmWave) channel models are also based on the rich scattering assumption. For example, the cluster fading envelope in [14]–[16] follows Rayleigh, while others [17]–[20] employ Rician fading distribution. Furthermore, fading studies [21]–[25] of directional line-of-sight (LOS) and non-LOS links show that Rx signal magnitude statistics are in good agreement with the Rician fading Rx envelope. Zöchmann *et al.* [26] demonstrated that the two-wave with diffuse power (TWDP) model is more suitable than the Rician fading model. The major difference between the Rice and TWDP fading model is that the former assumes a single fixed amplitude path, whereas the later assumes two paths. Romero-Jerez *et al.* [27] proposed fluctuating two-ray (FTR) model based on the experimental data in [22]. Note that, FTR model generalizes the TWDP model by introducing random fluctuations in both fixed amplitude paths. Similar to Rayleigh–Rice fading channels, both TWDP and FTR models represent rich scattering environment due to the circularly symmetric complex Gaussian assumption on the scattered MPCs.

Manuscript received June 19, 2018; revised November 9, 2018; accepted January 5, 2019. Date of publication January 23, 2019; date of current version April 5, 2019. *(Corresponding author: Naveed Iqbal.)*

N. Iqbal and J. Luo are with the Munich Research Center, Huawei Technologies Düsseldorf GmbH, 80992 Munich, Germany (e-mail: naveed.iqbal.q@gmail.com).

R. Müller, C. Schneider, S. Häfner, D. A. Dupleich, and R. S. Thomä are with the Electronic Measurements and Signal Processing Group, Technische Universität Ilmenau, 98693 Ilmenau, Germany.

G. Steinböck is with the Goteborg Research Center, Huawei Technologies, 41250 Gothenburg, Sweden.

Digital Object Identifier 10.1109/TAP.2019.2894277

[1] In general, Rayleigh–Rice fading models are used to describe both omnidirectional and multipath cluster fading channels. However, in this paper, they are discussed only to describe cluster fading statistics. In addition, in narrowband channels, a multipath cluster itself is often referred to as a resolvable MPC. However, in this paper, the terms like *MPCs, cissoids, and paths* always refer to intracluster MPCs. Finally, the term *channel* means only a group of MPCs corresponding to a multipath cluster unless otherwise stated as an *omnidirectional channel*.

[2] In literature, second-order fading statistics of the Rx envelope are described by temporal correlation functions, average fade duration (AFD) and level-crossing rate (LCR) of the Rx signal magnitude. However, studies in this paper are limited to the investigation of temporal correlation properties of the Rx signal. Motivations and detailed insights into each of the analyzed temporal correlation function are described in Section IV.

In contrast to the 3GPP-LTE systems [5], mmWave systems are supposed to operate with high gain antennas and high channel bandwidths. High gain antennas act as spatial filters for a propagation channel and a high bandwidth reduces smearing of MPCs in power delay profiles (PDPs). These features of mmWave systems may result in a sparse illumination of a cluster and radio channels (including antenna as a part of the channel) may appear as sparse multipath channels ($N < 10$). Note that the central limit theorem cannot be applied in sparse channels. Consequently, the statistical properties of a sparse multipath channel vary considerably from rich scattering channels as demonstrated in [28]–[30]. In particular, temporal correlation properties in [28] show that $\boldsymbol{Z}$ is a circularly symmetric non-Gaussian complex random variable for small N. Therefore, both $\boldsymbol{X}$ and $\boldsymbol{Y}$ cannot be modeled as statistically independent random processes [28]. Note that in a sparse multipath channel, the capacity of multiantenna systems scales sublinearly with a number of antenna elements [31]. Therefore, for accurate evaluations and predictions of mmWave system designs, fading assumptions and multipath modeling approaches in the standardized channel models such as 3GPP-TR 38.901 [14] need to be revised.

The main contribution of this paper is to show that when mmWave system features such as high bandwidth and/or beamforming gain are considered, then the conventional Rayleigh–Rice fading models for the cluster fading envelope may not be realistic. From hereinafter, the Rayleigh–Rice channels are jointly referred to as *reference models*. In contrast to the reference models, the temporal correlation properties of measured channels demonstrate that I and Q components of the Rx signal are highly correlated. Such properties explain that the measured multipath channels are sparse. Therefore, in the final part of this paper, a sum-of-cisoids (SOC)-based deterministic intracluster multipath modeling approach is proposed to reproduce the fading statistics of the measured mmWave channels. To the best of our knowledge, no such work exists in the mmWave channel modeling literature. Note that the same measurement data were used in our earlier work [24], [25], [32], but the presented insights in this paper are novel. The foundation of this paper is described by Pätzold and Rafiq [28], which provides a comprehensive study on theoretical differences between rich and sparse multipath channels.

The remainder of this paper is organized as follows. Details about the measurement campaign and the channel data processing are described in Sections II and III, respectively. In Section IV, the sparsity of intracluster multipaths is established through second-order statistical characterization of measured channels. Section V-A focuses on the extraction of parameters of interest, such as the standard deviation of the Rx signal magnitude around the local mean. These parameters are then used to derive SOC-based intra-cluster multipath modeling approach in Section V-B. Finally, conclusions are drawn in Section VI.

II. Scenario and the Channel Sounding Setup

Double-directional dual-band channel measurements are performed with a channel sounder which transmits a chip sequence of length 4095 with a chiprate of 6.75 GHz [33]. Channel sounder offers an instantaneous 3 dB absolute bandwidth of 4 GHz after calibration, where each frequency domain sample roughly corresponds to an absolute bandwidth of 2 MHz. The dynamic range of the channel sounder is up to 70 dB, which enables the identification of very weak MPCs. The measured channel impulse response (CIR) is post-processed by estimating a noise floor N_f (in decibels) using a procedure described in [34] and all time domain samples below $N_f + 10$ dB are zeroed out. Finally, a 25 dB dynamic range is applied to the CIR.

Fig. 1(a) shows a 360° panoramic view of a small lecture room at the Technische Universität Ilmenau campus. One of the inner brick made walls is covered by the metallic blackboards and the opposing wall is covered with 5 cm thick sound absorbers, whereas the outer wall has metallic frame windows. Doors and windows of the room are closed during measurements to ensure a static time-invariant propagation environment. The transmitter (Tx) is placed at a fixed position near the blackboard, whereby the Rx unit is placed on a rail with an initial 4.06 m distance between Tx and Rx, as shown in Fig. 1(a) and (b). In order to track changes in the time-varying radio channel, the Rx is moved in a certain direction with a step distance of Δx_s according to the setups shown in Fig. 1(c). To measure an aliasing-free Doppler power spectrum, Rx step distance should be at least two snapshots per wavelength λ_c of the center frequency f_c—i.e., $\Delta x_s \leq (\lambda_c/2)$ [35]. In this measurement campaign, the value $\Delta x_s = 2$ mm is maintained for both frequency bands which implies measuring 4 and 21 snapshots per wavelength at the mmWave and the FCC-ultrawideband, respectively. In this way, the chosen Δx_s guarantees aliasing-free Doppler power spectrum measurements for both the bands. A total measured distance from the first to the last Tx–Rx position is around 30 cm in each of four experimental setups shown in Fig. 1(c). The direction of Rx motion is same (i.e., away from Tx) for each measured radio channel setup; however, Tx and Rx antenna pointing angles may change depending upon the object being illuminated. As a result, Tx–Rx link distance increases/decreases with Rx movement as shown in Fig. 1(c). The height of both Tx and Rx units is around 1.68 m, which is approximately an eyesight height. Note that the Tx and Rx antenna center points are not perfectly aligned with each other as both are not placed right in front of or behind each other (on the same axis) as shown in Fig. 1(b). Due to this misalignment in the Tx–Rx axis, additional reflections from other objects in the room such as chairs and tables are also possible along with reflections from the intended surface.

For both FCC and mmWave bands, dual-polarized Tx–Rx horn antennas each with a 3 dB half-power beamwidth (HPBW) of 30° are used; further details are shown in Table I. During the measurements, different reflection surfaces are illuminated such that the intersection area of 3 dB Tx–Rx antenna footprints is around 3.4 m^2 on the surface. This intersection area imitates a multipath cluster referred to as geometry-based cluster in the literature [36]. Geometry-based clusters imitate a physical interacting object (IO) for MPCs in a realistic environment. On the other hand, conventional

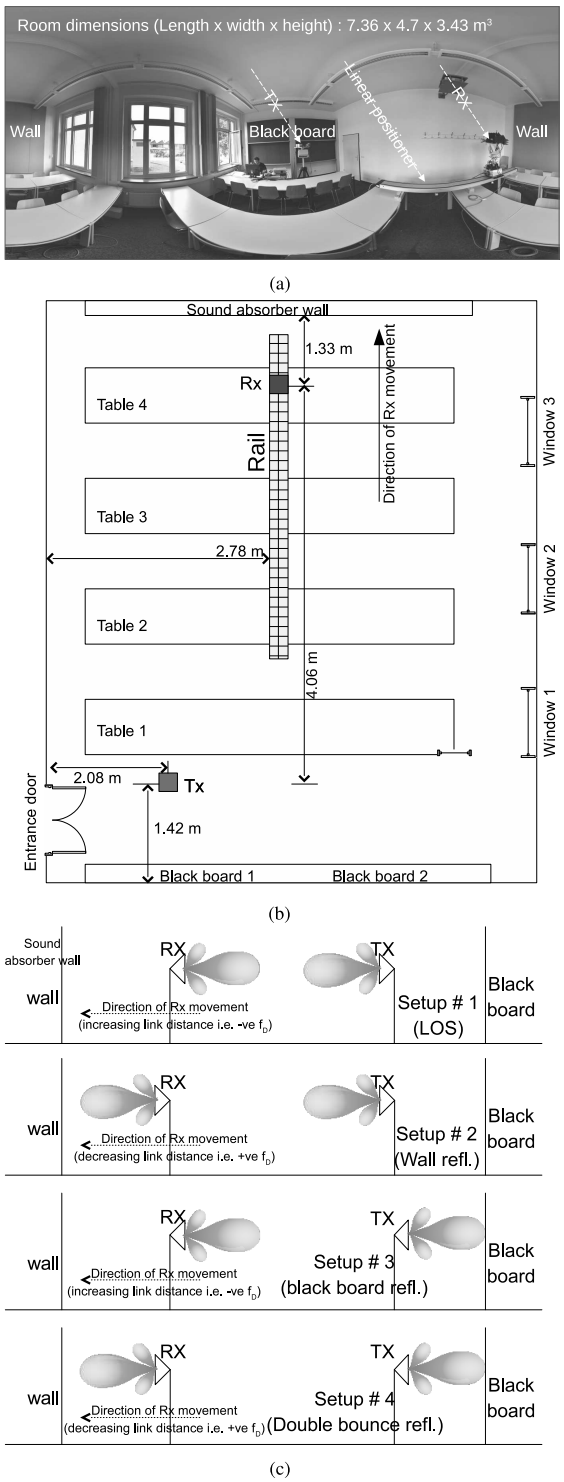

Fig. 1. Measurement scenario of small lecture room H-1519 at TU Ilmenau campus and double-directional measurement setups. Note that the *wall* considered in these experiments is a sound absorbing wall. (a) 360° panoramic view. (b) Overview of Tx–Rx positions. (c) Overview of Tx–Rx antenna pointing angles.

parameter-based clusters are based on the similarity of multipath channel parameters such as their time-delay, departure, and arrival angles. Parameter-based clusters do not necessarily correspond to a particular IO in an environment and much of their accuracy depends upon the applied multipath clustering algorithm. Furthermore, extraction of parameter-based clusters

TABLE I
CHANNEL SOUNDING AND MEASUREMENT PARAMETERS

Parameters	Values
Center frequency (f_c)	7 and 34 GHz
Average antenna XPD	30-35 dB
Measured bandwidth	3 dB absolute bandwidth of 4 GHz
Antenna HPBW	30°
Antenna gain	11-12 dBi
Initial Tx-Rx distance	4.06 m
Measured distance on the rail	30 cm
Rx movement step size	2 mm

requires array measurements, which is not the case here. We used 30° HPBW antennas as a compromise between low- and high-directive antennas due to the following reasons.

1) Decreasing antenna gain, e.g., to omnidirectional antennas may result in MPC contributions from a wide angular spread, thus violating the cluster definition.[3] Therefore, additional filtering in the delay and space domain would be required.
2) Very high gain antennas, in the worst case, may illuminate only a single MPC and not a group of MPCs to introduce small scale fading. In such a case, if a single path is illuminated, there would be no random process to model.

III. CHANNEL DATA PROCESSING

Let $H^{ab}(t, f)$ be the wideband channel transfer function (CTF) when a signal is transmitted with a polarization a and received with a polarization b, where $a, b \in \{H, V\}$. We assume that the directional CTF is frequency flat, which is quite plausible assumption as e directional antennas illuminate only the selective objects in particular directions, hence resulting in very low delay spread values and a large coherence bandwidth. Let n_f denote the total number of the frequency samples in the CTF at a particular time instant t, then

$$H^{ab}(t, f) = \sum_{n=1}^{n_f} A^{ab}(t, n) e^{j\theta^{ab}(t,f)} \delta(f - n\Delta f) \qquad (1)$$

where A^{ab} and θ^{ab} are the magnitude and phase responses of the channel at the nth frequency bin of the CTF at a time instant t. For the bandwidth reduction (if required), frequency domain samples are extracted while maintaining f_c and length of the full-band frequency domain channel in following way:

$$H_W^{ab}(t, f) = \begin{cases} H^{ab}(t, f), & f_l \le f \le f_h \\ 0 & \text{otherwise.} \end{cases} \qquad (2)$$

Now, the channel absolute bandwidth W is defined as $W = f_h - f_l$, where f_h and f_l are the highest and lowest frequencies of the band, respectively. Let τ be the time delay of an MPC, then the time domain CIR vector $h_W^{ab}(t, \tau)$ is obtained by the inverse Fourier transform of $H_W^{ab}(t, f)$. Fig. 2 shows some example PDPs of CIRs (without noise floor removal)

[3]We follow the most general definition of a multipath cluster—i.e., a group of MPCs propagating together in delay and space domains having similar departure and arrival angles.

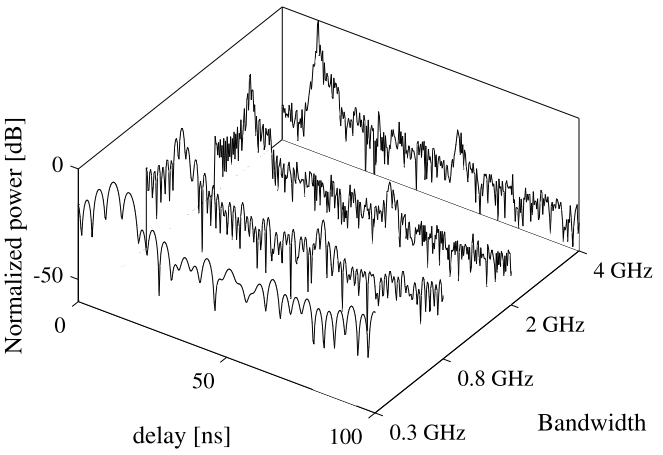

Fig. 2. CIR for various absolute bandwidths in setup # 1 (LOS case) for mmWave band, HH polarization setup. Note that each PDP is normalized locally to its peak power level i.e., $\sup\{P_W^{ab}(\tau)\}$.

for different channel bandwidths. These PDPs clearly show a reduction in the multipath smearing with an increase in the channel bandwidth. Consequently, high-bandwidth channels are sparse as compared to narrowband channels.

IV. Second-Order Statistical Characterization of Measured Channels

In general, second-order fading statistics are characterized by statistical functions known as LCR and AFD [9], [37]. Since our objective is to verify the circular symmetric complex Gaussian assumption associated with the Rx signal of the reference models, therefore investigations in this section are restricted to temporal correlation properties of measured multipath channels.

A. Temporal Autocorrelation Function

Now, we analyze the differences between the temporal autocorrelation functions (ACF) of measured channels and the reference model. Let f_D be a Doppler shift in an MPC received at a time delay τ, then the Doppler-variant impulse response $h_W^{ab}(\tau, f_D)$ is Fourier transform of $h_W^{ab}(\tau, t)$ along time t. Let $h_W^{ab}(\tau, t)$ be widesense stationary (WSS) in t, then the Doppler power spectral density (PSD) is defined as

$$\Phi_{\boldsymbol{h}}(f_D) = \int_0^{\infty} \left|h_W^{ab}(\tau, f_D)\right|^2 d\tau. \tag{3}$$

Let $\boldsymbol{h}(t)$ denote a random sample of the measured multipath channel at a time instant t, then the temporal ACF $c_{\boldsymbol{h}}(\Delta t) = E\{\boldsymbol{h}(t)\boldsymbol{h}^*(t + \Delta t)\}$[4] is equivalent to the inverse Fourier transform of $\Phi_{\boldsymbol{h}}(f_D)$. For $\Delta t > 0$, the absolute value of $c_{\boldsymbol{h}}(\Delta t)$ quantifies the channel coherence time (or distance) and its knowledge plays a key role in channel tracking algorithms [38]. For the reference model, $c_{\boldsymbol{h}}(\Delta t) = J_0(2\pi f_{\max}\Delta t)$ is a real-valued function having a symmetric U-shaped Doppler PSD, where J_0 is a zeroth-order Bessel function of first kind and $f_{\max}$ is the maximum Doppler frequency. However, $c_{\boldsymbol{h}}(\Delta t)$ in realistic channels is expected to be a complex-valued function with asymmetric Doppler PSDs which are caused either by nonisotropic scattering from the propagation environment or by use of directional antennas as shown in Fig. 3.[5] Clearly, the ACFs of measured multipath clusters differ considerably from the reference model. For the FCC band, a high similarity between the Doppler PSDs (and ACFs) shows that the impact of surface scattering is not very significant. For the wall and double bounce reflections, a comparison of Doppler PSDs of both bands shows that

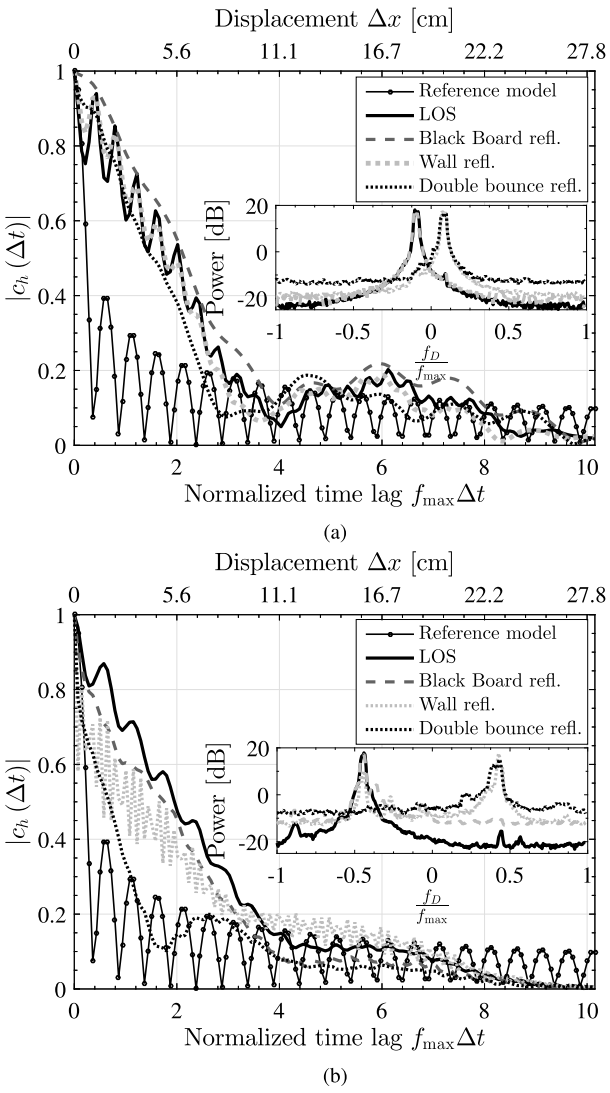

Fig. 3. Analysis of ACF for different reflection surfaces, VV polarization, $f_{\max} = 100$ Hz, $W = 4$ GHz. Speed of the Rx is equal to 10 km/h. Recalling that the measurements do not consider a highly controlled environment such that MPCs are received only from an intended reflection surface. Therefore, in some measurements, an abuse of multipath cluster definition (same delay and the same AoA of MPCs) is possible. (a) FCC band. (b) mmWave.

[4] $(\cdot)^*$ denotes the complex conjugate of the function.

[5] Note that comparisons shown in Figs. 3 and 4 consider same absolute bandwidth (W) for both FCC and mmWave frequency bands. Similar comparisons with same relative bandwidth may also provide an interesting insight into the fading statistics. For example, due to increased smearing of MPCs, we expect that fading statistics of clusters at the FCC band would be comparatively closer to the reference models.

TABLE II
CORRELATION DISTANCE IN TERMS OF WAVELENGTH FOR DIFFERENT CLUSTERS

	LOS	Black board refl.	Wall refl.	Double bounce refl.	Rayleigh/ Rice
FCC band	$1.3\lambda_c$	$1.4\lambda_c$	$1.3\lambda_c$	$1\lambda_c$	$0.1\lambda_c$
mmWave band	$6.1\lambda_c$	$5.5\lambda_c$	$5.2\lambda_c$	$2\lambda_c$	$0.7\lambda_c$

a number of peaks[6] in the mmWave band are higher than FCC band. These observations are in-line with the hypothesis in [39], which states that smaller wavelengths at mmWave frequencies may lead to more diffuse scattering than lower frequency bands. Assuming that a channel is correlated if $|c_{\boldsymbol{h}}(\Delta t)| \geq 0.5$, results in Table II summarize correlation distances in measured channels. One may note that, for the mmWave band, the correlation distances for different measurement setups differ considerably from each other, whereby they are quite similar for FCC band. This observation clearly demonstrates that the influence of surface scattering at the correlation distance is more pronounced in the mmWave band than the FCC band.

B. Temporal Cross Correlation and Complementary Autocorrelation Functions

Now, we aim to analyze sparsity of intra-cluster multipaths in the measured channels. For that, temporal cross correlation function (CCF) $\gamma_{IQ}(t_1, t_2) = E\{\Re(\boldsymbol{h}(t_1))\Im(\boldsymbol{h}^T(t_2))\}$ is studied, which measures correlation between real ($\Re$) and imaginary ($\Im$) components of the channel. Recalling that a vanishing CCF $\gamma_{IQ}(\Delta t) \approx 0, \forall \Delta t \geq 0$ explains that Rx signal is a complex Gaussian random variable which corresponds to a rich scattering channel and vice versa. In addition, for both FCC and mmWave bands, a comparative analysis is done to investigate if the measured Rx signal is a circularly symmetric complex random variable or not. This is analyzed by the complementary ACF (CACF), i.e., $r_{\boldsymbol{h}}(t_1, t_2) = E\{\boldsymbol{h}(t_1)\boldsymbol{h}^T(t_2)\}$, which measures correlation between $\boldsymbol{h}(t)$ and its complex conjugate $\boldsymbol{h}^*(t)$. A channel $\boldsymbol{h}(t)$ is said to be the second-order stationary, if it is WSS and the CACF is only a function of Δt [40]. The propagation channel $\boldsymbol{h}(t)$ with a vanishing CACF $r_{\boldsymbol{h}}(\Delta t) \approx 0, \forall \Delta t \geq 0$ is a circularly symmetric complex random variable [40]. Assuming that $\boldsymbol{h}(t)$ is second-order stationary, then the real and imaginary parts of $r_{\boldsymbol{h}}(\Delta t)$ are defined as

$$\Re\{r_{\boldsymbol{h}}(\Delta t)\} = \mu_{II}(\Delta t) - \mu_{QQ}(\Delta t) \tag{4}$$

and

$$\Im\{r_{\boldsymbol{h}}(\Delta t)\} = \gamma_{IQ}(\Delta t) + \gamma_{QI}(\Delta t) \tag{5}$$

where $\mu_{II}(\Delta t)$ and $\mu_{QQ}(\Delta t)$ are the ACFs of I and Q components, respectively. Note that, in case of a circularly symmetric complex Gaussian signal, $\mu_{II}(\Delta t) = \mu_{QQ}(\Delta t)$ and $\gamma_{IQ}(\Delta t) = \gamma_{QI}(\Delta t) = 0$, resulting in $r_{\boldsymbol{h}}(\Delta t) = 0, \forall \Delta t \geq 0$. However, every circularly symmetric signal is not always a complex Gaussian random variate. In fact, $r_{\boldsymbol{h}}(\Delta t) = 0$ also when $\mu_{II}(\Delta t) = \mu_{QQ}(\Delta t)$ and $\gamma_{IQ}(\Delta t)$ is a nonzero odd function [41]. A nonzero CACF establishes the following facts: 1) the second-order statistics have not been fully described by $c_{\boldsymbol{h}}(\Delta t)$ and 2) the channel $\boldsymbol{h}(t)$ is a noncircular or improper complex vector [42]. In this case, beamforming techniques based on the widely linear processing result in higher performance gains over the linear counterparts [42].

Fig. 4 shows that both $\gamma_{IQ}(\Delta t)$ and $r_h(\Delta t)$ are roughly equal to zero at $\Delta t = 0$, which explains that I and Q components of the Rx signal are (instantaneously) mutually uncorrelated. However, $\gamma_{IQ}(\Delta t) \neq 0$ for $\Delta t > 0$ and as such differs from the reference model. For $\Delta t > 0$, Fig. 4(c) and (d) shows that the values of $\gamma_{IQ}(\Delta t)$ are higher for FCC than the mmWave band. This observation indicates that wall and double bounce clusters when illuminated with FCC band are sparser than mmWave band demonstrating an increased surface scattering at the mmWave band. Similarly, for the mmWave band, LOS, and blackboard clusters are sparser than the wall and double bounce reflections. This is due to the reduced scattering in LOS and black-board clusters as compared to the wall and double-bounce reflections, which agrees with the intuition and from the Doppler PSDs in Fig. 3. Nonzero CCFs in Fig. 4 imply that the rich scattering assumption made in the Rayleigh, Rice, TWDP, and FTR fading models is not satisfied. For all $\Delta t > 0$, the results $\gamma_{IQ}(\Delta t) \neq 0$ and $r_{\boldsymbol{h}}(\Delta t) \approx 0$ demonstrate that $\mu_{II}(\Delta t) = \mu_{QQ}(\Delta t)$ and $\gamma_{IQ}(\Delta t)$ is an odd function. As such, we conclude that the complex Rx signal is a circularly symmetric non-Gaussian random variable with a rotationally invariant probability distribution function (PDF). These properties are in agreement with correlation properties of sparse channels in [28]. From the system performance perspectives, in this case, both linear and its widely linear beamforming counterpart will result in similar performances [42].

Here, it is important to emphasize that in narrowband channels, the amplitude of $\gamma_{IQ}(\Delta t)$ decreases but does not vanish to zero due to the asymmetry of the Doppler PSD. The Rx envelope will then converge toward the reference model [43]. The presented results and discussions above lead to the following remark. With limited bandwidth (narrowband assumption) at lower frequency bands, the reference model assumption as used in 3GPP-TR 38.901 [14] and WINNER [7] is valid and sufficient. However, the reference model is not realistic when it comes to: 1) larger bandwidth even at bands below 10 GHz and 2) mm-wave bands with traditionally higher bandwidths.

V. PARAMETERIZATION AND MULTIPATH MODELING OF MEASURED CHANNELS

In this section, from the measurements, we first extract the parameters required for the intra-cluster multipath modeling. After that, an SOC-based deterministic multipath modeling approach is proposed.

A. Parameter Extraction From Measured Channels

1) Mean Value: We normalize the CTF $H_W^{ab}(t, f)$ such that the ensemble average of the time-varying Rx signal

[6]By *peaks*, we mean the number of ripples in the Doppler PSDs shown in Fig. 3 which corresponds to the intracluster scattered MPCs.

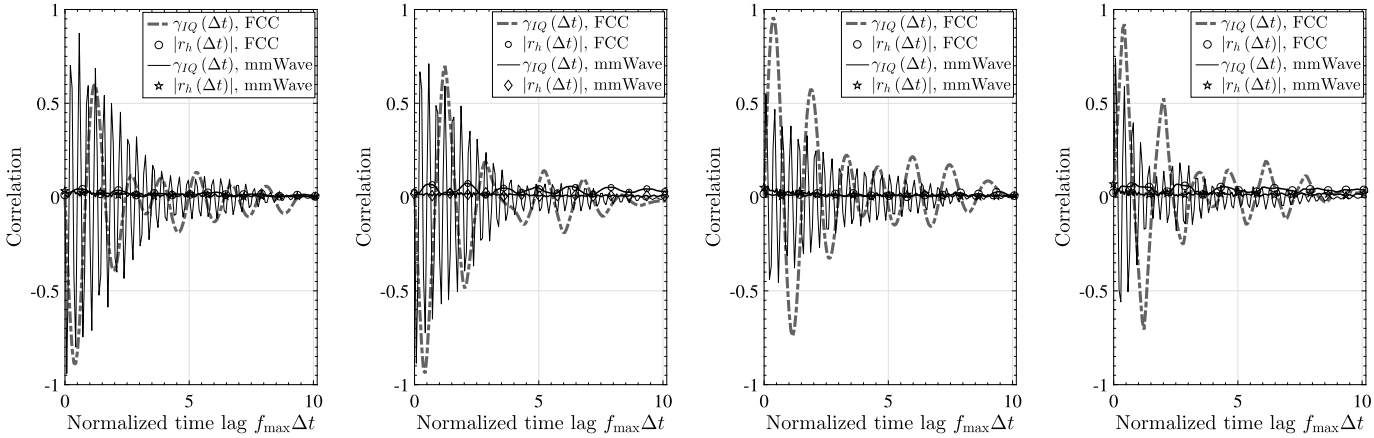

Fig. 4. Analysis of CACF and the CCF for different measurement setups, VV antenna polarization setup, $f_{\max} = 100$ Hz, $W = 4$ GHz. Speed of the Rx is equal to 10 km/h. (a) LOS. (b) Black board refl. (c) Wall refl. (d) Double bounce refl.

magnitude $m_{\mathrm{Rx}}(t)$ is

$$\rho = E\{m_{\mathrm{Rx}}(t)\} = 1 \tag{6}$$

where, from the Parseval's relation

$$m_{\mathrm{Rx}}(t) = \sqrt{\int_0^\infty \left|h_W^{ab}(t,\tau)\right|^2 d\tau} = \sqrt{\int_{-\infty}^\infty \left|H_W^{ab}(t,f)\right|^2 df}. \tag{7}$$

This normalization removes the global pathloss (due to an initial Tx–Rx distance) in each measurement. However, the local pathloss or path gain effect due to the movement afterward on the rail is maintained which introduces a Doppler shift in MPCs. In addition, the normalization in (6) implies that the mean value of the $m_{\mathrm{Rx}}(t)$ remains constant, irrespective of the bandwidth and the measurement setup.

2) Standard Deviation (σ_0): The standard deviation characterizes the variations in the magnitude of the Rx signal. The results shown in Fig. 5 compare σ_0 as a function of W. It can be observed that σ_0 differs considerably in different propagation setups implying a strong influence of scattered MPCs in defining the cluster fading behavior.

Intuitively, depending upon a propagation scenario, σ_0 should decrease up to a particular bandwidth W_0 known as stability bandwidth[7] [1]. An increase in bandwidth beyond W_0 does not result in a considerable change in Rx signal fading statistics and the value of σ_0. Therefore, a dual slope regression fit is quite intuitive and it results in a reasonably good approximation. Higher order polynomials may provide a better approximation, but the slope-constant model in (8) is proposed to maintain simplicity and intuitiveness

$$\sigma_0^{ab}(W) = \begin{cases} c_0 - m\log_{10} W, & \text{if } W \le W_0 \\ c_1 & \text{otherwise.} \end{cases} \tag{8}$$

In (8), the bandwidth W is in gigahertz, the slope m describes the rate of descent in $\sigma_0^{ab}(W)$, constant c_0 is the average amplitude of I/Q components of plane waves in narrow-band channels and c_1 is their amplitude at the stability bandwidth W_0. Table III shows the parameter values of the model in (8) for copolarized and cross-polarized measured channels.

[7]*Stability bandwidth* corresponds the system bandwidth at which most of MPCs in the channel are resolved. Therefore, an increase in bandwidth beyond W_0 does not cause any significant variations in the fading envelope.

It is interesting to note that on average c_0 has higher values in case of wall reflections, demonstrating a large amplitude fading in narrow-band channels. However, the slope factor m is also higher than other propagation setups, demonstrating a relatively faster convergence toward nonfading regime with an increase in W. The reason behind this observation is that MPCs are relatively well separated in the delay domain in case of wall reflections than other measured channel setups. Consequently, intracluster MPCs are resolved more quickly with W resulting in higher values of m. The mean square error (MSE) between measurements and the model in (8) is calculated as

$$\xi = \sum_{i=1}^{n_{\mathrm{B}}} \left(\underbrace{\sigma_0^{ab}(W_i)}_{\text{model in (8)}} - \underbrace{\tilde{\sigma}_0^{ab}(W_i)}_{\text{est. from measurements}} \right)^2 \tag{9}$$

where n_{B} corresponds to a total number of bandwidth samples. Table III shows the normalized MSE (ξ_n), computed by normalizing ξ in (9) by $\sum_{i=1}^{n_{\mathrm{B}}} \tilde{\sigma}_0^{ab}(W_i)$. Very small values of the MSE in Table III show a good agreement between measurements and the model in (8).

B. Intracluster Multipath Modeling of Measured Channels

We now use the parameters (mean and standard deviation) extracted in the earlier Section V-A to model intracluster multipath attenuation gains c_n and total number of scattered MPCs N per cluster. Multipath modeling methodologies in the state-of-the-art channel models can be mainly classified into *deterministic* and *stochastic* parameter computation methods as shown in Table IV. In a deterministic method, gains c_n and AoAs (or Doppler frequencies f_n) are set to a fixed value within a small scale fading area (drop duration). Different snapshots of the channel are then generated only by the uniform random variation of multipath phases θ_n. In contrast, with a stochastic method, each channel snapshot is generated by a random combination of c_n, AoAs, and multipath phases. Given a certain theoretical reference model, the accuracy of the deterministic method improves by increasing N, while the stochastic method requires exhaustive channel sounding measurements for reliable statistics of multipath parameter estimates. In addition, estimates of c_n and N are largely

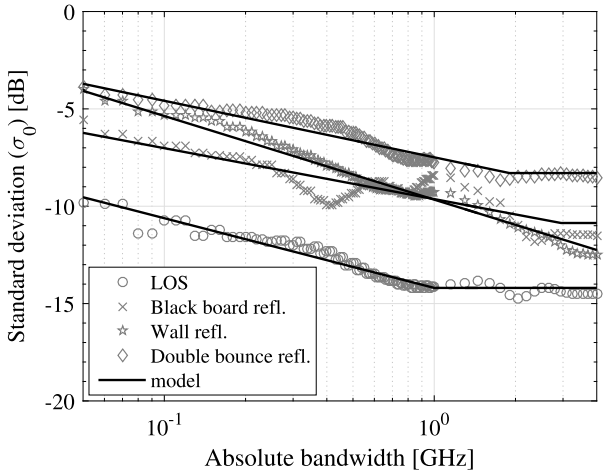

Fig. 5. Standard deviation (σ_0) of the received signal magnitude as a function of channel absolute bandwidth, mmWave band, VV polarization.

TABLE III

PARAMETER VALUES FOR EMPIRICAL MODEL OF AVERAGE DIFFUSE MPCS AMPLITUDES AS A FUNCTION OF BANDWIDTH

		LOS	Black board refl.	wall refl.	double bounce refl. (Wall and black board)
VV	m	3.6	2.7	4.3	2.9
	c_0	18	15	29	18.6
	c_1	-14.2	-11.3	-12.2	-8.3
	W_0	1 GHz	3 GHz	4 GHz	2 GHz
	$\log_{10}(\xi_n)$	-3.2	-2.3	-2.8	-2.5
HH	m	2.8	1.7	3.2	1.7
	c_0	12.3	7.1	18.2	8
	c_1	-12.7	-9.5	-10.5	-8.4
	W_0	1 GHz	1 GHz	1 GHz	1 GHz
	$\log_{10}(\xi_n)$	-2.5	-2.2	-1.8	-2
VH	m	2.5	2	3.5	3.1
	c_0	14.3	12.2	22.4	21.1
	c_1	-9.2	-6.7	-11	-8.8
	W_0	2 GHz	2 GHz	4 GHz	2 GHz
	$\log_{10}(\xi_n)$	-2	-1.4	-2.3	-3

limited by the delay resolution of the channel sounder. More discussions on stochastic and deterministic parameter computation methods can be found in [44] and [45].

Intracluster MPC modeling approach in this paper is based on the deterministic parameter computation method. Analysis of correlation properties in Section IV reveal that the intracluster MPC structure is sparse in measured channels. Consequently, the measured Rx envelope will not closely follow the reference model. Therefore, we consider PDF of the measured Rx signal magnitude as a performance benchmark. We use the SOC simulation model [43], as it inherently assumes that I and Q components of Rx signal envelope are correlated for small N. This is not the case for classical sum-of-sinusoids (SOS) model proposed earlier by Clarke [10] and Jakes and Cox [48]. Of course, one can modify the classical SOS principle to generate correlated I and Q components as in the SOC simulator which is a subclass of the SOS model. As $N \to \infty$, both SOC and SOS simulators result in the reference model distribution with (roughly) uncorrelated I and Q

TABLE IV

CLASSES OF INTRACLUSTER MPC MODELING METHODOLOGY AND CHANNEL MODELS CORRESPONDING TO EACH CLASS

Parameter computation method	Model
Deterministic method (Constant c_n, constant Doppler frequencies[a] and random phases)	3GPP-TR 38.901 [14]
	mmMAGIC [15]
Properties: Mean and auto-correlation ergodic [9]	METIS-2020 [16]
	WINNER II [7]
	3GPP SCM [6]
Stochastic method (Random c_n, Random Doppler frequencies[b] and random phases)	IEEE 802.11 ad/ay [17], [18]
	Conf. room model [19]
	MiWEBA [20]
Properties: Mean ergodic, non-ergodic auto-correlation [9]	Extended Saleh-Valenzuala model [46]
	NYU [47]

[a]The models [6], [7], [14]–[16] do not explicitly model Doppler spectrum. However, fixed intra-cluster MPC AoA assignments from the cluster Power-Angular-Spectrum demonstrate constant Doppler frequencies of sinusoids per snapshot. Note that mmMAGIC and METIS channel models have focused largely at the fast fading parametrization for the 3GPP standardization activities while maintaining the intra-cluster MPC modeling methodology.

[b]Models [17]–[20], [46] consider that intra-cluster AoAs are randomly distributed within a cluster angular spread. NYU [47] assumes MPC clustering in the delay domain only, and MPC may arrive only from certain directions in space known as spatial lobes. Random intra-cluster MPC AoAs per snapshot demonstrate random Doppler frequencies of sinusoids.

components. Let ρ, f_ρ, and θ_ρ be the gain, Doppler frequency, and phase of the LOS/dominant path, then a nonzero mean SOC random process is defined as

$$Z(t) = \rho e^{j(2\pi f_\rho t + \theta_\rho)} + \sum_{n=1}^{N} c_n e^{j(2\pi f_n t + \theta_n)}. \tag{10}$$

Absolute value $|Z(t)|$ in (10) defines the envelope process. Assuming that c_n and f_n are the constant entities and θ_n is independent identically distributed random process, then by taking into account that I and Q components of Rx envelope are correlated, the PDF of an SOC process becomes [9, Eq. (4.120)]

$$p_Z(r) = (2\pi)^2 r \int_0^\infty \left[\prod_{n=1}^{N} J_0(2\pi |c_n| x)\right] \cdot J_0(2\pi r x) J_0(2\pi \rho x) x dx, \quad N \geq 1 \tag{11}$$

where r is the Rx signal magnitude. Due to the correlated I and Q assumption, the PDF in (11) can provide a nice fit to the PDF of measured Rx envelope for small N. However, this requires extensive evaluation of (11) for $N \geq 1$ and comparison with the PDF of the measured Rx envelope. These evaluations are driven by the parameters ρ and σ_0 extracted from the measurements in Section V-A. During the evaluation of (11), mean value defined by the non-centrality parameter ρ of the distribution is fixed to $\rho = 0$ dB due to the normalization in (6). Constant amplitudes of N scattered MPCs are plugged in (11) as following: 1) $c_n = \sigma_0\sqrt{2/N}$, i.e., equal amplitude sinusoids or 2) $c_n = \mathcal{R}\sqrt{\sigma_0^2/N}$, i.e., Rayleigh distributed amplitude of sinusoids. Note that the second moment parameter σ_0 in c_n establishes a connection between

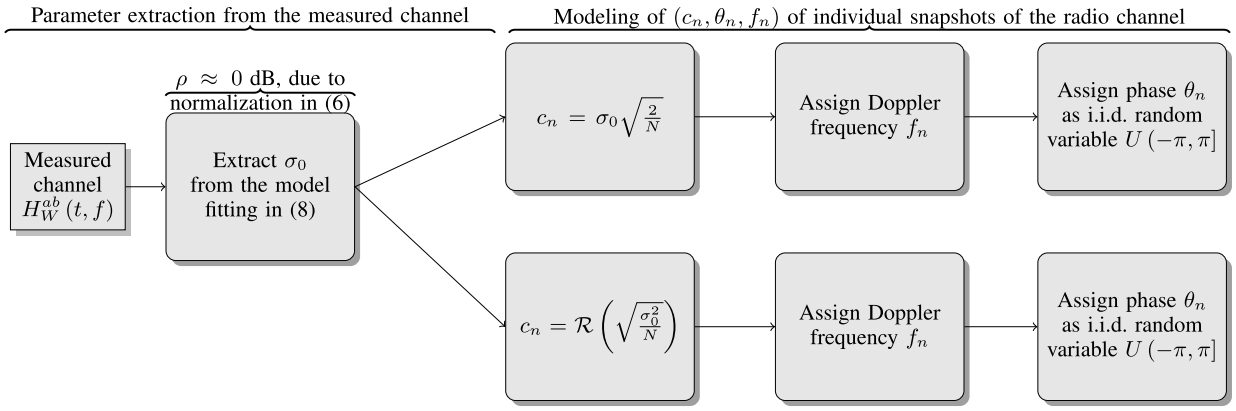

Fig. 6. Intracluster multipath modeling process with deterministic parameter computation methods.

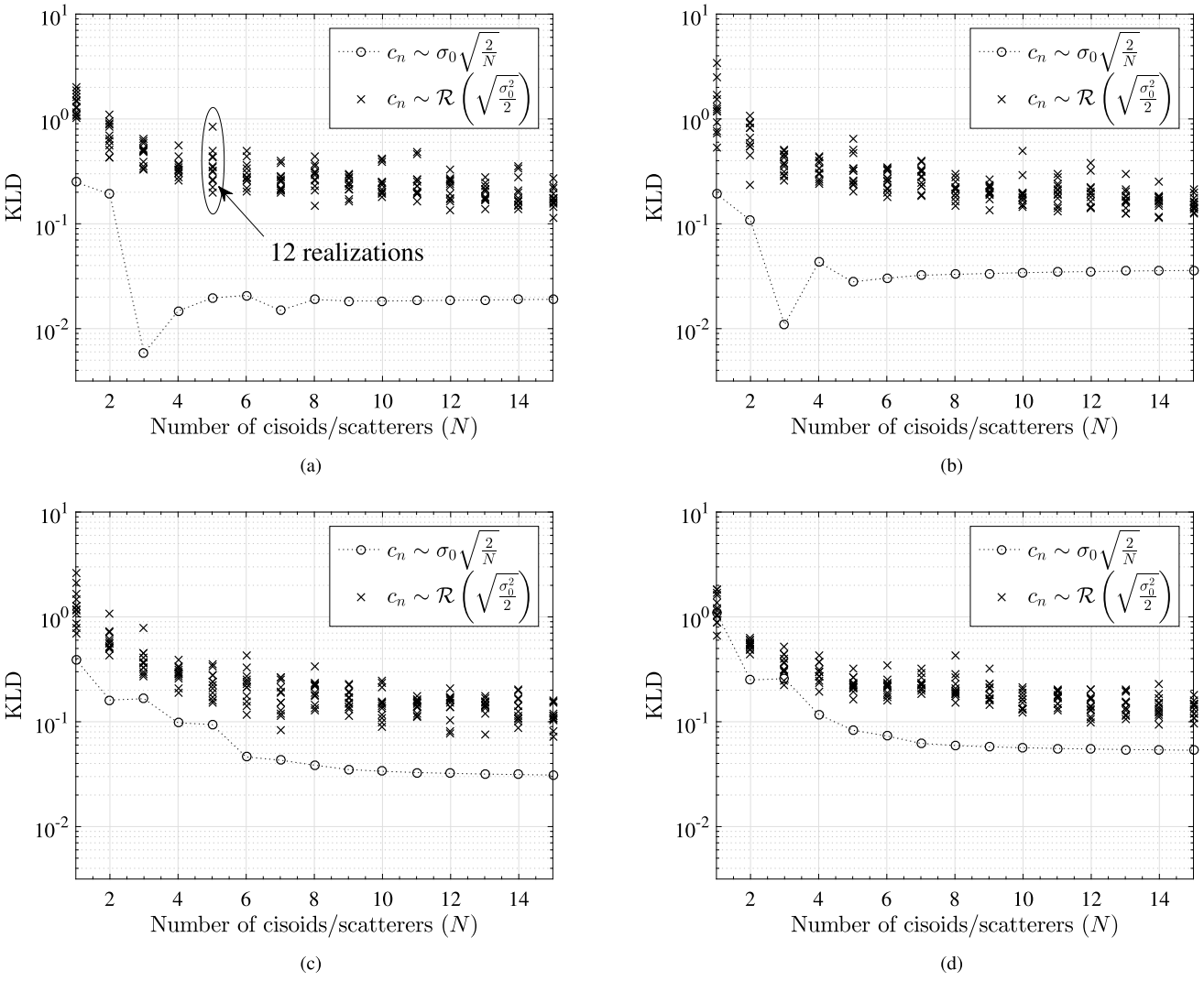

Fig. 7. Analysis of KLD versus N, mmWave band, σ_0 is obtained by using the model in (8), $\rho = 0$ dB, VV polarization, $W = 4$ GHz. (a) LOS. (b) Black board reflection. (c) Wall reflections. (d) Double bounce reflections.

measurements and the multipath modeling. From (11), it is clear that the PDF of Rx envelope does not depend upon the Doppler frequency or AoA of an MPC. Therefore, modeling of f_n is not considered in this paper. Fig. 6 summarizes the steps of our proposed deterministic multipath modeling methodology.

Let P and Q be the probability mass functions of the measured Rx envelope and the PDF in (11), respectively. The relative entropy $D_{KL}(P \parallel Q)$ as known as Kullback–Leibler distance (KLD) quantifies a distance between P and Q [49]

$$D_{KL}(P \parallel Q) = \sum_r P(r) \log\left(\frac{P(r)}{Q(r)}\right). \tag{12}$$

Since $D_{KL}(P \parallel Q)$ may not be equal to $D_{KL}(Q \parallel P)$, a symmetric metric is built by taking the average of two opposite KLDs in the following way:

$$D_{\bar{KL}}(P \parallel Q) = \frac{1}{2}[D_{KL}(P \parallel Q) + D_{KL}(Q \parallel P)]. \quad (13)$$

A convergence of KLD in (13) toward zero demonstrates that the probability mass functions P and Q are in close agreement with each other.

If $c_n = \sigma_0\sqrt{2/N}$, then results in [43] show that (11) provides a very good approximation of the reference model for $N \geq 10$. However, when $c_n = \mathcal{R}(\sqrt{\sigma_0^2/N})$, results in [28] show that (11) converges to the reference model for $N \geq 50$. These results form the basis of our analysis in Fig. 7 where symmetric KLDs for both deterministic MPC amplitude modeling approaches are compared for different N. Due to the stochastic nature of $c_n = \mathcal{R}(\sqrt{\sigma_0^2/N})$, results from 12 different realizations of c_n are plotted for each N. If $c_n = \sigma_0\sqrt{2/N}$, results in Fig. 7(a) and (b) demonstrates that (11) provides an excellent approximation of Rx envelope at $N = 3$. However, KLD increases again for $N > 3$, i.e., when (11) converges toward the reference model. This explains that the measured Rx envelope does not closely follow the reference model. For LOS and black board reflections, these results are theoretically expected due to considerably higher cross correlation values in Fig. 4(a) and (b) and the sparse scattering shown by Doppler PSDs in Fig. 3(b). In narrowband channels, Rx envelope will converge toward the reference model due to an increased smearing of the intracluster MPCs. From Fig. 7(a) and (b), one may argue that the KLD between the measured Rx envelope predicted by (11) and the reference model is not large enough. We emphasize that when the system considers single Tx–Rx antenna elements, channel correlation properties show major differences between sparse and rich scattering channels as demonstrated in Section IV. Similar results are evident in all measured channels at the 7 GHz frequency band due to considerably high cross correlation values shown in Fig. 4.

Considering again that $c_n = \sigma_0\sqrt{2/N}$, the case of wall and double-bounce reflections in Fig. 7(c) and (d) shows that (11) provides the best approximation of the measured Rx envelope $\forall N \geq 10$. Small KLD values indicate that the measured Rx envelope is in good agreement with the reference model. However, the KLD does not approach toward zero with an increase in N. This is due to the existence of nonzero CCFs shown in Fig. 4(c) and (d), which is not a case in the reference model. These results also indicate that SOC simulation model becomes sensitive at lower cross correlation values. From Fig. 7, it is also clear that Rayleigh distributed scattered MPC amplitudes does not provide a better approximation of the measured Rx envelope than equal amplitude MPCs.

VI. Discussion and Conclusion

Investigation of temporal correlation properties and Doppler PSDs in this paper shows that the intracluster number of MPCs are quite low for both FCC and mmWave band. This multipath sparsity depends on the bandwidth and/or beamforming gain with which a system illuminates a multipath cluster. As the rich scattering assumption is not satisfied, the cluster fading envelope does not closely follow the Rayleigh–Rice fading envelope. This shows that, for the cluster fading envelope, the use of Rayleigh–Rice fading distributions in the models [14]–[20] is not realistic. In fact, cluster fading distributions with a single nonfluctuating path along with $N = 3 - 6$ equal amplitude scattered MPCs provide a considerably good but not an optimal approximate of the measured Rx magnitude.

The empirical bandwidth-dependent model proposed in this paper explains that the standard deviation (or fading depth) of the cluster fading envelope vanishes exponentially with an increase in the channel bandwidth and as shown in [3] with the antenna gain. Using the same measurement campaign, results reported earlier in [32] show that the randomness in the cross-polarization power ratio vanishes exponentially with the bandwidth. In other words, randomness in the 2×2 polarization coupling matrix also vanishes with the bandwidth. This demonstrates that, due to their wider bandwidths and/or beamwidths, mmWave systems will experience reduced/no small scale fading. In contrast, 3GPP-TR 38.901 [14] model demonstrates a high-Rx signal magnitude fading, first due to the Rayleigh fading assumption on the cluster, and second due to the polarization coupling matrix which is modeled as random even in the large bandwidth extension.

Results also show that the temporal correlation properties and correlation distances for different clusters are quite similar to each other for the FCC band, but differ considerably in the mmWave band. This shows that mmWave bands are more sensitive to the type of reflection surfaces than the FCC band. In contrast, the fading envelope of all clusters in 3GPP-TR 38.901 [14] model is Rayleigh distributed, irrespective of any frequency band in range 0.5–100 GHz.

The presented results motivate us to study the multipath clusters in outdoor channels, where the cluster to the Rx distance could be much larger than in indoor channels. In addition, more rough surfaces as reflecting objects need to be investigated along with investigations at higher frequency bands.

Acknowledgment

The authors would like to thank Dr. W. Q. Malik from the Massachusetts Institute of Technology, USA, Dr. G. Rafiq from the University of Agder, Norway, and Dr. M. Boban for the fruitful discussions that the authors had during this work.

References

[1] M. V. Clark and L. J. Greenstein, "The relationship between fading and bandwidth for multipath channels," *IEEE Trans. Wireless Commun.*, vol. 4, no. 4, pp. 1372–1376, Jul. 2005.

[2] W. Q. Malik, B. Allen, and D. J. Edwards, "Fade depth scaling with channel bandwidth," *Electron. Lett.*, vol. 43, no. 24, pp. 1371–1372, Nov. 2007.

[3] D. Dupleich *et al.*, "Investigations on fading scaling with bandwidth and directivity at 60 GHz," in *Proc. 11th Eur. Conf. Antennas Propag. (EuCAP)*, Mar. 2017, pp. 3375–3379.

[4] A. F. Molisch, "Ultra-wide-band propagation channels," *Proc. IEEE*, vol. 97, no. 2, pp. 353–371, Feb. 2009.

[5] *Evolved Universal Terrestrial Radio Access (E-UTRA) Physical Channels and Modulation*, 3rd Generation Partnership Project (3GPP), Standard 36.211 V10.2.0, 2011.

[6] "Spatial channel model for multiple input multiple output (MIMO) simulations," 3rd Gener. Partnership Project, Tech. Rep. 25.996, version 12.0.0, Release 12, 2014.
[7] P. Kyösti *et. al.*, "WINNER II channel models," Eur. Commission, Tech. Rep. IST-4-027756, Sep. 2007.
[8] W. B. Davenport, Jr., and W. L. Root, *An Introduction to the Theory of Random Signals and Noise*, vol. 159. New York, NY, USA: McGraw-Hill, 1958.
[9] M. Pätzold, *Mobile Radio Channels*. Hoboken, NJ, USA: Wiley, 2011.
[10] R. H. Clarke, "A statistical theory of mobile-radio reception," *Bell Syst. Tech. J.*, vol. 47, no. 6, pp. 957–1000, Jul. 1968.
[11] C. Loo, "A statistical model for a land mobile satellite link," *IEEE Trans. Veh. Technol.*, vol. VT-34, no. 3, pp. 122–127, Aug. 1985.
[12] H. Suzuki, "A statistical model for urban radio propogation," *IEEE Trans. Commun.*, vol. COMM-25, no. 7, pp. 673–680, Jul. 1977.
[13] M. Nakagami, "The *m*-distribution—A general formula of intensity distribution of rapid fading," in *Statistical Methods in Radio Wave Propagation*. Amsterdam, The Netherlands: Elsevier, 1960, pp. 3–36.
[14] "Study on channel model for frequencies from 0.5 to 100 GHz," 3rd Gener. Partnership Project, Tech. Rep. 38.901, V1.0.1, Mar. 2017.
[15] M. Peter *et al.*, "Measurement results and final mmMAGIC channel models," document H2020-ICT-671650-mmMAGIC/D2.2, Deliverable D2.2, 2017.
[16] V. Nurmela *et al.*, *Deliverable D1.4 METIS Channel Models*, document ICT-317669-METIS/D1.4, Mobile and wireless communications Enablers for the Twenty-twenty Information Society, 2015, p. 1.
[17] A. Maltsev *et al.*, *Channel Models for 60 GHz WLAN Systems*, IEEE Standard 802.11-09/0334r8, 2010.
[18] A. Maltsev, A. Pudeyev, A. Lomayev, and I. Bolotin, "Channel modeling in the next generation mmWave Wi-Fi: IEEE 802.11ay standard," in *Proc. 22nd Eur. Wireless Conf.*, May 2016, pp. 1–8.
[19] C. Gustafson, K. Haneda, S. Wyne, and F. Tufvesson, "On mm-wave multipath clustering and channel modeling," *IEEE Trans. Antennas Propag.*, vol. 62, no. 3, pp. 1445–1455, Mar. 2014.
[20] A. Maltsev, *Channel Modeling and Characterization—MiWEBA*, document Deliverable 5.1 EU Contract no. FP7-ICT-608637, 2014.
[21] S. Sun, H. Yan, G. R. MacCartney, and T. S. Rappaport, "Millimeter wave small-scale spatial statistics in an urban microcell scenario," in *Proc. IEEE Int. Conf. Commun. (ICC)*, May 2017, pp. 1–7.
[22] M. K. Samimi, G. R. MacCartney, S. Sun, and T. S. Rappaport, "28 GHz millimeter-wave ultrawideband small-scale fading models in wireless channels," in *Proc. IEEE 83rd Veh. Technol. Conf. (VTC Spring)*, May 2016, pp. 1–6.
[23] D. Dupleich *et al.*, "Influence of system aspects on fading at mm-waves," *IET Microw., Antennas Propag.*, vol. 12, no. 4, pp. 516–524, Mar. 2017. [Online]. Available: http://digital-library.theiet.org/content/journals/10.1049/iet-map.2017.0601
[24] N. Iqbal *et al.*, "On the stochastic and deterministic behavior of mmWave channels," in *Proc. 11th Eur. Conf. Antennas Propag. (EuCAP)*, Mar. 2017, pp. 1813–1817.
[25] N. Iqbal, C. Schneider, J. Luo, D. Dupleich, R. Müller, and R. S. Thomä, "Modeling of directional fading channels for millimeter wave systems," in *Proc. IEEE 86th Veh. Technol. Conf. (VTC-Fall)*, Sep. 2017, pp. 1–5.
[26] E. Zöchmann *et al.* (2018). "Better than Rician: Modelling millimetre wave channels as two-wave with diffuse power." [Online]. Available: https://arxiv.org/abs/1804.03417
[27] J. M. Romero-Jerez, F. J. Lopez-Martinez, J. F. Paris, and A. J. Goldsmith, "The fluctuating two-ray fading model: Statistical characterization and performance analysis," *IEEE Trans. Commun.*, vol. 16, no. 7, pp. 4420–4432, Jul. 2017.
[28] M. Pätzold and G. Rafiq, "Sparse multipath channels: Modelling, analysis, and simulation," in *Proc. IEEE 24th Annu. Int. Symp. Pers., Indoor, Mobile Radio Commun. (PIMRC)*, Sep. 2013, pp. 30–35.
[29] R. Hicheri, M. Pätzold, and N. Youssef, "On the statistical properties of the capacity of sparse multipath fading channels," in *Proc. Int. Conf. Adv. Technol. Commun. (ATC)*, Oct. 2014, pp. 338–343.
[30] N. Iqbal *et al.*, "Second-order statistical characterization of the 60 GHz cluster fading channels," in *Proc. IEEE 29th Annu. Int. Symp. Pers., Indoor Mobile Radio Commun. (PIMRC)*, Sep. 2018, pp. 241–245.
[31] V. Raghavan and A. M. Sayeed, "Sublinear capacity scaling laws for sparse MIMO channels," *IEEE Trans. Inf. Theory*, vol. 57, no. 1, pp. 345–364, Jan. 2011.
[32] N. Iqbal *et al.*, "Stochastic/deterministic behavior of cross polarization discrimination in mmWave channels," in *Proc. IEEE ICC Wireless Commun. Symp. (ICC WCS)*, May 2017, pp. 1–5.
[33] R. Müller *et al.*, "Simultaneous multi-band channel sounding at mm-wave frequencies," in *Proc. 10th Eur. Conf. Antennas Propag. (EuCAP)*, Apr. 2016, pp. 1–5.
[34] A. Böttcher, C. Schneider, P. Vary, and R. S. Thomä, "Dependency of the power and delay domain parameters on antenna height and distance in urban macro cell," in *Proc. 5th Eur. Conf. Antennas Propag. (EUCAP)*, Apr. 2011, pp. 1395–1399.
[35] A. F. Molisch, *Wireless Communications*, 2nd ed. Hoboken, NJ, USA: Wiley, 2011.
[36] M. Zhu, "Geometry-based radio channel characterization and modeling: Parameterization, implementation and validation," Ph.D. dissertation, Dept. Elect. Inf. Technol., Lund Univ., Lund, Sweden, 2014.
[37] P. Vasconcelos and L. M. Correia, "Fading characterization of the mobile radio channel at the millimetre waveband," in *Proc. IEEE 47th Veh. Technol. Conf. Technol. Motion*, vol. 2, May 1997, pp. 999–1003.
[38] X. Gao, L. Dai, Y. Zhang, T. Xie, X. Dai, and Z. Wang, "Fast channel tracking for terahertz beamspace massive MIMO systems," *IEEE Trans. Veh. Technol.*, vol. 66, no. 7, pp. 5689–5696, Jul. 2017.
[39] A. F. Molisch *et al.*, "Millimeter-wave channels in urban environments," in *Proc. 10th Eur. Conf. Antennas Propag. (EuCAP)*, Apr. 2016, pp. 1–5.
[40] B. Picinbono and P. Bondon, "Second-order statistics of complex signals," *IEEE Trans. Signal Process.*, vol. 45, no. 2, pp. 411–420, Feb. 1997.
[41] F. D. Neeser and J. L. Massey, "Proper complex random processes with applications to information theory," *IEEE Trans. Inf. Theory*, vol. 39, no. 4, pp. 1293–1302, Jul. 1993.
[42] P. J. Schreier and L. L. Scharf, *Statistical Signal Processing of Complex-Valued Data: The Theory of Improper and Noncircular Signals*. Cambridge, U.K.: Cambridge Univ. Press, 2010.
[43] M. Pätzold and B. Talha, "On the statistical properties of sum-of-cisoids-based mobile radio channel models," in *Proc. WPMC*, 2007, pp. 394–400.
[44] M. Pätzold, U. Killat, F. Laue, and Y. Li, "On the problems of Monte Carlo method based simulation models for mobile radio channels," in *Proc. Symp. IEEE 4th Int Spread Spectr. Techn. Appl.*, vol. 3, Sep. 1996, pp. 1214–1220.
[45] Y. R. Zheng and C. Xiao, "Improved models for the generation of multiple uncorrelated Rayleigh fading waveforms," *IEEE Commun. Lett.*, vol. 6, no. 6, pp. 256–258, Jun. 2002.
[46] Q. H. Spencer, B. D. Jeffs, M. A. Jensen, and A. L. Swindlehurst, "Modeling the statistical time and angle of arrival characteristics of an indoor multipath channel," *IEEE J. Sel. Areas Commun.*, vol. 18, no. 3, pp. 347–360, Mar. 2000.
[47] M. K. Samimi and T. S. Rappaport, "3-D millimeter-wave statistical channel model for 5G wireless system design," *IEEE Trans. Microw. Theory Techn.*, vol. 64, no. 7, pp. 2207–2225, Jul. 2016.
[48] W. C. Jakes and D. C. Cox, Eds., *Microwave Mobile Communications*. Hoboken, NJ, USA: Wiley, 1994.
[49] T. M. Cover and J. A. Thomas, *Elements of Information Theory*. Hoboken, NJ, USA: Wiley, 2012.

Naveed Iqbal (S'17) received the B.Sc. degree in electronics from Quaid-e-Azam University, Islamabad, Pakistan, in 2008, and the M.Sc. degree in communications and signals processing from Technische Universität Ilmenau, Ilmenau, Germany, in 2014. He is currently pursuing the Ph.D. degree with the German Research Center, Huawei Technologies Düsseldorf GmbH, Munich, Germany.

He has been involved in the mmMAGIC project. He has contributed to the development of mmMAGIC, IEEE 802.11ay, and 3GPP TR 37.885 channel models. He is currently involved in channel models for millimeter-wave systems. His current research interests include channel measurements and modeling for mm-wave communication systems, low-complexity deterministic/randomized algorithms for antenna subset selection and beamforming techniques for MIMO systems.

Mr. Iqbal was a recipient of two best research paper awards at the European Wireless Conference in 2013 and the European Conference on Antennas and Propagation in 2017.

Jian Luo received the B.Sc. degree in communications engineering from the South China University of Technology, Guangzhou, China, in 2004, and the M.Sc. and Ph.D. degrees in electrical engineering from Technische Universität Berlin, Berlin, Germany, in 2006 and 2012, respectively.

From 2007 to 2012, he was a Researcher with the Fraunhofer Heinrich Hertz Institute, Berlin, where he was involved in several German national and EU funded projects, including EASY-A, SMART-RF, and SAPHYRE. Since 2012, he has been with the German Research Center, Huawei Technologies Düsseldorf GmbH, Munich, Germany, where he has been involved in 5G wireless communication systems. He has been involved in EU H2020 5GPPP METIS, mmMAGIC, 5GCAR, and 5G-VINNI projects. In mmMAGIC, he led the air-interface design. His current research interests include channel measurement and modeling, 5G system, especially millimeter wave, and 5G for V2X/vertical industry.

Robert Müller received the M.S. degree in electronic engineering from the Berlin University of Technology, Berlin, Germany, in 2009.

His current research interests include high-frequency components design, high-frequency front-end design, antenna design, ultrawideband system design, and special antenna array design for channel sounding applications, channel sounding measurements system and analysis for a further communication system in the field of V2V and cellular networks.

Gerhard Steinböck received the Dipl.-Ing. (FH) degree in telecommunications from Technikum Wien, Vienna, Austria, in 1999, and the M.Sc.E. *(cum laude)* and Ph.D. degrees in wireless communications from Aalborg University, Aalborg, Denmark, in 2008 and 2013, respectively.

He was a Post-Doctoral Researcher with Aalborg University. From 2000 to 2006, he was a Research and Development Engineer with the Austrian Institute of Technology, Vienna, Austria, where he was contributing, among other things, to the hardware and software development of a real-time radio channel emulator. In 2016, he joined Huawei Technologies Sweden AB, Gothenburg, Sweden. His current research interests include wireless communications, systems simulation, radio channel modeling, radio channel estimation and sounding, and radio geolocation techniques.

Christian Schneider received the Diploma degree in electrical engineering from Technische Universität Ilmenau, Ilmenau, Germany, in 2001, where he is currently pursuing the Ph.D. degree with the Institute for Information Technology.

His current research interests include wireless multidimensional channel sounding, channel characterization and analysis, channel modeling for single-link and multilink cases in cellular and vehicular networks at microwave and millimeter-wave bands, space–time signal processing, adaptive techniques, and passive coherent localization.

Mr. Schneider was a recipient of the Best Paper Award at the European Wireless Conference in 2013 and the European Conference on Antennas and Propagation in 2017.

Diego Andres Dupleich received the engineering degree in electronic engineering from Universidad Tecnológica Nacional, Paraná, Argentina, in 2009, and the M.Sc. degree (Hons.) in communications and signal processing from Technische Universität Ilmenau, Ilmenau, Germany, in 2013, where he is currently pursuing the Ph.D. degree in millimeter-wave systems and radio channel measurements/modeling with the Electronic Measurement Research Laboratory.

Mr. Dupleich was a recipient of the Best Paper Award in the 11th European Conference on Antennas and Propagation (EuCAP 2017).

Stephan Häfner received the M.Sc. degree in computer engineering from Technische Universität Ilmenau (TU Ilmenau), Ilmenau, Germany, in 2012, where he is currently pursuing the Ph.D. degree.

Since 2012, he has been with the Electronic Measurement Research Laboratory, TU Ilmenau. His current research interests include array signal processing and high-resolution parameter estimation for channel sounding and radar applications.

Reiner S. Thomä (M'92–SM'99–F'07) received the Dipl.-Ing. (M.S.E.E.), Dr.-Ing. (Ph.D.E.E.), and Dr.-Ing. habil. degrees in electrical engineering and information technology from Technische Universität Ilmenau (TU Ilmenau), Ilmenau, Germany, in 1975, 1983, and 1989, respectively.

From 1975 to 1988, he was a Research Associate with TU Ilmenau, where he was involved in electronic circuits, measurement engineering, and digital signal processing. From 1988 to 1990, he was a Research Engineer with the Center for Scientific Instrument Engineering, German Academy of Sciences at Berlin, Berlin, Germany, where he was involved in radio surveillance. In 1991, he spent a sabbatical leave with the Department of Communications Engineering, University of Erlangen–Nuremberg, Erlangen, Germany. Since 1992, he has been a Professor of electrical engineering (electronic measurement) with TU Ilmenau, where he was the Director of the Institute of Communications and Measurement Engineering from 1999 to 2005. With his group, he has contributed to several European and German research projects and clusters such as RESCUE, WINNER, PULSERS, EUWB, NEWCOM, COST 273, 2100, IC 1004, COSR IRACON, EASY-A, and EASY-C. He was the Speaker of the German Nation-Wide DFG-Focus Project UKoLOS, Ultra-Wideband Radio Technologies for Communications, Localization, and Sensor Applications (SPP 1202). His current research interests include measurement and digital signal processing methods (correlation and spectral analysis, system identification, sensor arrays, compressive sensing, and time–frequency and cyclostationary signal analysis), their application in mobile radio and radar systems (multidimensional channel sounding, propagation measurement and parameter estimation, MIMO-, mm-wave-, and ultrawideband radar), measurement-based performance evaluation of MIMO transmission systems including over-the-air testing in virtual electromagnetic environments, passive coherent location, and UWB radar sensor systems for object detection, tracking, and imaging.

Dr. Thomä is a member of URSI (Comm. A), VDE/ITG. He was an Advisory Board Member of EU project—mmMAGIC. He has been the Chair of the IEEE-IM TC-13 on Measurement in Wireless and Telecommunications since 1999. He was a recipient of the Thuringian State Research Award for Applied Research both for contributions to high-resolution multidimensional channel sounding in 2007 and the Vodafone Innovation Award in 2014.